10.1098/rsta.2000.0752

THE ROYAL SOCIETY

Frictional chatter in orthogonal metal cutting

By Marian Wiercigroch[1] and Anton M. Krivtsov[2]

[1]*Department of Engineering, King's College, University of Aberdeen, Aberdeen AB24 3UE, UK*

[2]*Department of Theoretical Mechanics, St. Petersburg State Technical University, St. Petersburg, Russia*

A comprehensive study of the frictional chatter occurring during metal-cutting process is given. A general mathematical model of the machine-tool–cutting process is established, and then a high-accuracy numerical algorithm is developed. Next, a two-degree-of-freedom model of orthogonal metal cutting is examined. Then stochastic properties of the material being cut are introduced to reflect variations in the workpiece properties, in particular, in the cutting resistance. Nonlinear dynamics techniques, such as constructing bifurcation diagrams and Poincaré maps, are employed to ascertain dynamics responses for both the deterministic and the stochastic model. Untypical routes to chaos and unusual topology of Poincaré cross-sections are observed. The conducted analysis has provided some practical design recommendations. Finally, occurrence of chatter was investigated analytically.

Keywords: machine-tool chatter; dry friction; orthogonal metal cutting; nonlinear dynamics

1. Introduction

Large relative vibrations between the tool and the workpiece in metal-cutting processes can compromise the productivity and accuracy of this manufacturing technique. This is particularly dangerous when a sudden and uncontrolled rise of vibration amplitude occurs. In many practical situations, the conditions in which such a instability appears can be satisfactorily explained by linear dynamics. However, more comprehensive insight can be gained only if the dynamic interactions between the machine tool (MT) and the cutting process (CP) are treated as nonlinear. An example of such behaviour is self-excited oscillations, so-called chatter.

Despite the continuing effort in the field, and generation of new theories, there is no consistent explanation for the existence of chatter. The fundamental reason behind it is the complexity of the chip-formation process, where the following strongly nonlinear phenomena are interrelated and dependent: temperature-dependent plasticity; temperature- and velocity-dependent friction; nonlinear stiffness of machine tools; regenerative effects; and intermittency of the cutting process. There are two different types of chatter: primary and secondary. Primary chatter is caused mainly by the variable shear stresses in the primary and secondary plastic deformation zones, and the frictional effects of the chip acting on the rake surface due to the relative motion between the workpiece and tool. Secondary chatter is predominantly an outcome of the regenerative effects, where the workpiece geometry from the previous pass influences the dynamics of the next pass (e.g. Stépán 1998).

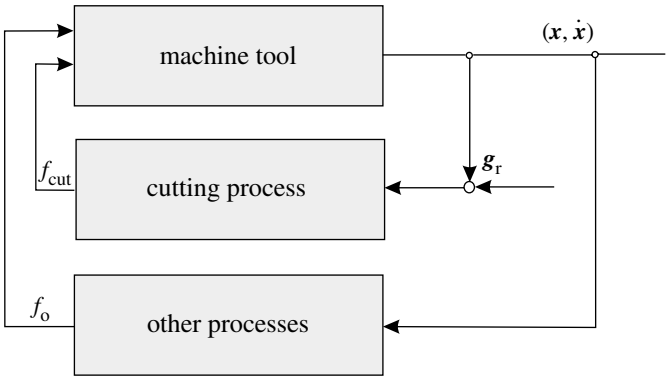

Figure 1. Diagram showing dynamic interactions during a metal-cutting process.

The most influential work on the dynamics of machine tools and cutting processes was conducted in the mid forties by Merchant (1944, 1945), and later, in the 1950s and 1960s, by Russians. The studies conducted by Zorev (1956) and Kudinov (1963a, b) are good examples of those investigations, where the dynamics characteristics of the cutting process play a key role in process stability. Contrary to this approach, there is a significant body of research assuming that the machine-tool structure is responsible for the dynamic instabilities (e.g. Tlusty 1986).

Recent investigations into nonlinear dynamics have shown an existence and importance of chaotic motion occurring in machining. The models by Grabec (1988), Wiercigroch (1997), Wiercigroch & Cheng (1997) and Foong *et al.* (2001) have shown evidence of chaotic vibrations, which are mainly due to the nonlinearity of the dry friction and the intermittent contact between the cutting tool and the workpiece.

The main goal of this paper is to study simple models which describe the dynamic interactions in the uncoupled MT–CP system. Modern nonlinear dynamic techniques, such as constructing bifurcation diagrams and Poincaré maps, will be employed to ascertain the dynamic behaviour. A broad programme of numerical simulation will be carried out in order to map regions of parameters where different types of motion occur. The paper will conclude with the stability analysis for a single-degree-of-freedom model, providing a guide of how to choose the system and technological parameters in order to avoid frictional chatter.

2. Dynamic interactions within the MT–CP system

Dynamics of any mechanical system including machine tools can be described by the following second-order differential equation,

$$\frac{\partial^2 \boldsymbol{x}}{\partial t^2} = \boldsymbol{f}\left(t; \boldsymbol{x}, \frac{\partial \boldsymbol{x}}{\partial t}, \boldsymbol{p}\right), \tag{2.1}$$

where $\boldsymbol{x}(t)$ is the displacement vector, $\boldsymbol{p}$ is the system-parameters vector and $\boldsymbol{f}(\cdot)$ is the force vector, dependent on both the internal and external excitations. In our case, the vector $\boldsymbol{f}(\cdot)$ comprises the structural force between different elements of the machine tool, $\boldsymbol{f}_{\mathrm{str}}(\boldsymbol{x}, \dot{\boldsymbol{x}})$, the cutting force $\boldsymbol{f}_{\mathrm{cut}}(\boldsymbol{x}, \dot{\boldsymbol{x}})$, and the external noise force $\boldsymbol{f}_{\mathrm{en}}$.

The MT–CP system may be treated as a dynamic system with a feedback control, which is schematically depicted in figure 1. During the chip formation, the vector of cutting force, $\boldsymbol{f}_{\mathrm{cut}}$, is generated and acts with the vector of other forces, $\boldsymbol{f}_{\mathrm{o}}$, on the machine-tool structure. In the absence of noise ($\boldsymbol{f}_{\mathrm{en}} = \boldsymbol{0}$), the required geometry, $\boldsymbol{g}_{\mathrm{r}}$, is distorted by the relative vibrations between the tool and the workpiece, which can be represented by the vector $(\boldsymbol{x}, \dot{\boldsymbol{x}})$.

Let us consider a machine-tool structure with n degrees of freedom, and express the cutting force explicitly. Equation (2.1) takes the following form (Wiercigroch 1990),

$$\boldsymbol{m}\ddot{\boldsymbol{x}} + \boldsymbol{c}(\dot{\boldsymbol{x}})\dot{\boldsymbol{x}} + \boldsymbol{k}(\boldsymbol{x})\boldsymbol{x} = \boldsymbol{f}_{\mathrm{cut}}(\boldsymbol{x}, \dot{\boldsymbol{x}}) - \boldsymbol{t}(\dot{\boldsymbol{x}}), \tag{2.2}$$

where $\boldsymbol{m}$, $\boldsymbol{c}(\cdot)$ and $\boldsymbol{k}(\cdot)$ are the mass, viscous damping and stiffness matrices, respectively, $\boldsymbol{x}$, $\dot{\boldsymbol{x}}$ and $\ddot{\boldsymbol{x}}$ are the generalized displacement, velocity and acceleration, respectively, and $\boldsymbol{f}_{\mathrm{cut}}(\cdot)$ is the cutting force. A practical example of such a system is a rough hole-boring process on a horizontal-boring and milling machine (Wiercigroch 1990), where the geometric accuracy of the process is achieved via a kinematic coordination of the spindle rotation with the axial motion of the table.

The cutting process is highly nonlinear and also parametric, as some of the parameters vary with time (e.g. the spindle stiffness). The cutting force is proportional to the cross-sectional area of the layer being cut. This area can be calculated by knowing the change of the geometric vector, $\Delta\boldsymbol{g}$, which, in turn, can be evaluated from the formula

$$\Delta\boldsymbol{g} = \Phi\boldsymbol{x} + \Delta\boldsymbol{g}_{\mathrm{in}}, \tag{2.3}$$

where Φ is the transformation matrix and $\Delta\boldsymbol{g}_{\mathrm{in}}$ is the dynamic change of the input vector. Thus the expression for the dynamic cutting force can be written as follows,

$$\boldsymbol{f}_{\mathrm{cut}} = \boldsymbol{w}(\boldsymbol{g})\Delta\boldsymbol{g} + \boldsymbol{h}(\dot{\boldsymbol{g}})\Delta\dot{\boldsymbol{g}}, \tag{2.4}$$

where $\boldsymbol{w}(\boldsymbol{g})$ is the cutting-process amplification matrix and $\boldsymbol{h}(\dot{\boldsymbol{g}})$ is the damping effect. One of the most essential tasks in nonlinear dynamic analysis is numerical integration of the equations of motion. In particular, if the considered system has motion-dependent discontinuities, any imprecision in integration can generate false solutions. This is well known—the collocation methods are regarded as one of the best as far as computational accuracy is concerned (Hillber & Hughes 1978); however, these methods require so-called *restart*, i.e. the calculation of the acceleration vector at each time-step. If the vector of external force is given explicitly, the restart process is straightforward, and the acceleration vector is given as (Wiercigroch 1994)

$$\boldsymbol{a}_{k+1} = \boldsymbol{M}_{k+1}^{-1}(\boldsymbol{F}_k + \boldsymbol{F}_{k+1}). \tag{2.5}$$

As can be seen, equation (2.5) is written in a form resembling Newton's second law, where $\boldsymbol{a}_{k+1}$ is the acceleration vector, $\boldsymbol{M}_{k+1}$ is the equivalent inertia matrix, and $\boldsymbol{F}_k$ and $\boldsymbol{F}_{k+1}$ are the equivalent external forces calculated for the k and $k+1$ time-step, respectively,

$$\boldsymbol{M}_{k+1} = (\Theta s)^2(0.5-\beta)\boldsymbol{w}\Phi + \Theta s\gamma\boldsymbol{h}\Phi - (\Theta\boldsymbol{m} + \Theta s\gamma\boldsymbol{c} + (\Theta s)^2\beta\boldsymbol{k}), \tag{2.6}$$

$$\begin{aligned}\boldsymbol{F}_k = [&(\Theta s)^2(0.5-\beta)\boldsymbol{w}\Phi + \Theta s(1-\gamma)\boldsymbol{h}\Phi \\ &- (1-\Theta)\boldsymbol{m}\Theta s(1-\gamma)\boldsymbol{c} + (\Theta s)^2(0.5-\beta)\boldsymbol{k}]\boldsymbol{a}_k \\ &- [\Theta s\boldsymbol{w}\Phi + \boldsymbol{h}\Psi - \boldsymbol{c} - \Theta s\boldsymbol{k}]\boldsymbol{v}_k + [\boldsymbol{w}\Phi - \boldsymbol{c}]\boldsymbol{d}_k - \boldsymbol{h}\Phi\boldsymbol{v}_{k-n} - \boldsymbol{w}\Phi\boldsymbol{d}_{k-n},\end{aligned} \tag{2.7}$$

$$\boldsymbol{F}_{k+1} = \boldsymbol{w}\Delta\boldsymbol{g}_{\mathrm{in},k+1} + \boldsymbol{h}\Delta\dot{\boldsymbol{g}}_{\mathrm{in},k+1}, \tag{2.8}$$

where s is the time-step, β, γ and Θ are the collocation parameters, $\boldsymbol{a}_k$, $\boldsymbol{v}_k$ and $\boldsymbol{d}_k$ are the acceleration, velocity and displacement vectors at the kth time-step, respectively, $\boldsymbol{v}_{k-n}$ and $\boldsymbol{d}_{k-n}$ are the velocity and displacement vectors at the $(k-n)$th time-step, and $T = n$ s is the period of one spindle revolution. The example given above is particularly relevant to the dynamic interactions occurring in the rough hole-boring process, which gives a flavour of the complexity of the problem. Moreover, the described procedure proved to be very effective in accurate calculation of the dynamic responses for nonlinear multi-degree-of-freedom systems.

A rigorous mathematical treatment of the plastic deformation in the cutting zone and chip formation is still far from satisfactory. Therefore, most attention has been paid to the static relationships between kinematic and geometrical parameters of the cutting process, and the generated cutting forces. Let us assume steady-state conditions and consider a three-dimensional vector of the cutting force, $\boldsymbol{f}_{\mathrm{cut}}$, which is dependent on the changes of the cutting parameters α_j, the process constants c_j and β_j, and the Heaviside function $H_{j,l}$, to account for the separation between the tool and the workpiece. Thus the ith component of the cutting force can be evaluated from

$$\boldsymbol{f}_{\mathrm{cut},i} = \prod_{j=1}^{n} c_i \alpha_j^{\beta_{i,j}} H_{j,l}(\alpha_k), \quad i = 1,2,3, \quad l \in n, \quad l \leqslant k < n. \tag{2.9}$$

The cutting parameters α_j are functions of the displacement and velocity, and can be written symbolically as follows:

$$\alpha_j = g(\boldsymbol{x}, \dot{\boldsymbol{x}}). \tag{2.10}$$

3. Frictional and impact chatter in the two-degree-of-freedom model

(*a*) *Deterministic model*

The instantaneous separation of the cutting tool from the workpiece, namely an intermittent cutting process, has a great influence on the system dynamics. Therefore, our model of the MT–CP system should take into account the feedback control loop through $\boldsymbol{f}_{\mathrm{cut}}$, and also the discontinuity of the process. To concentrate on the nonlinear dynamics issues, a simple but realistic model of the MT–CP system will be considered. The elastic, dissipative and inertial properties of the machine-tool structure, tool and the workpiece are represented by a planar oscillator, which is excited by the cutting-force components f_x and f_y (see figure 2*a*). It is assumed that the relationship between the cutting forces and the chip geometry, namely the cutting-process characteristics, is captured by orthogonal cutting, where the cutting edge is parallel to the workpiece and normal to the cutting direction, as depicted in figure 2*b*. In our case, the cutting parameters α_j should be understood as the depth of cut, h, and the relative velocity, v_{r}. Due to vibration in the x-direction, the relative velocity v_{r} can cross the zero-value point; therefore, static and dynamic friction occurs. Thus the cutting-process characteristics, as a function of the relative velocity, cannot be expressed directly by (2.9); therefore, one can postulate the following relationships,

$$f_x = c_x h^{\beta_x} H(h) g_x(v_{\mathrm{r}}), \tag{3.1}$$

$$f_y = c_y h^{\beta_y} H(h) g_y(v_{\mathrm{r}}), \tag{3.2}$$

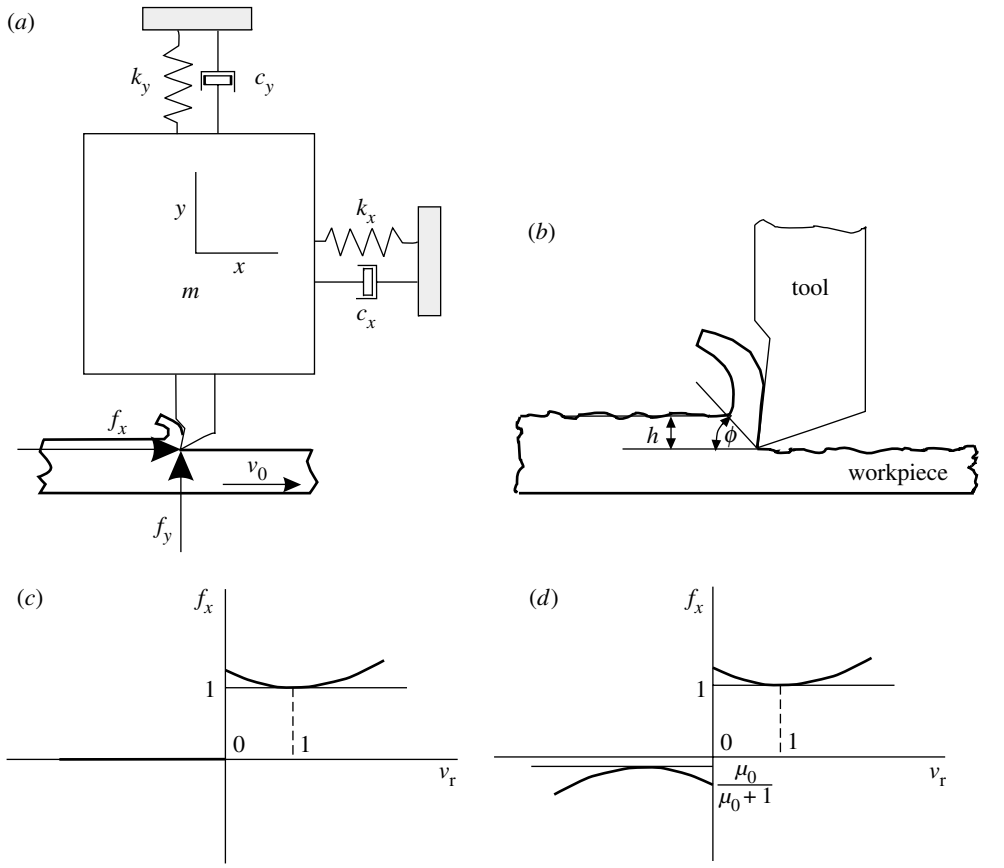

Figure 2. MT–CP system. (*a*) Physical model. (*b*) Chip geometry. (*c*) Former form of f_x. (*d*) New form of f_x as a function of the relative velocity v_r.

where the two unknown functions $g_x(v_r)$ and $g_y(v_r)$ need to be given explicitly. Since f_x and f_y are mutually related, one can be expressed by the other. This approach was adopted from Hastings *et al*. (1980), where the cutting forces for a wide class of technical materials are described by the following expressions,

$$f_x(y, x', y') = q_0 h(c_1(\mathrm{abs}(v_r) - 1)^2 + 1)H(h), \tag{3.3}$$

$$f_y(y, x', y') = \xi(v_r, v_f, h) f_x(y, x', y'), \tag{3.4}$$

where

$$\begin{aligned}
\xi &= (c_2(v_f - 1)^2 + 1)(c_3(h - 1)^2 + 1)H(f_x)\,\mathrm{sgn}(v_f),\\
v_r &= v_0 - x',\\
v_f &= v +_0 -Ry',\\
h &= h_0 - y,\\
R &= R_0(c_4(v_r - 1)^2 + 1).
\end{aligned}$$

It is assumed that the force, f_y, is mainly due to the friction, ξ, acting on the rake surface. The friction velocity, v_f, is reduced due to shear plastic deformation, R,

which is related to the shear angle, ϕ (see figure 2*b*),

$$R = \cot\phi. \tag{3.5}$$

The cutting process starts with an initial depth of cut, h_0, where a layer is taken from the workpiece with the constant velocity, v_0. Throughout the process it is assumed that the cutting parameters, such as $c_1, \ldots, c_4$ and q_0, are fixed. The non-linear relationship between the cutting force, f_x, and chip velocity is graphically presented in figure 2*c*, where, for $v_\mathrm{r} < 0$, the excitation force is equal to zero. In reality, this force never disappears completely as there is always a considerable friction force due to the compression force in the vertical spring. To make this approach more realistic, a dry friction force acting in x-direction for the $v_\mathrm{r} < 0$ cases needs to be added. On the other hand, equation (2.6) should still be valid to predict the total force, f_x, for the $v_\mathrm{r} \geqslant 0$ cases. A modified formula, which satisfies the conditions listed above, is written below and presented graphically in figure 2*d*,

$$f_x(y, x', y') = q_0 h\left(H(v_\mathrm{r})\frac{1}{1+\mu_0} + \mathrm{sgn}(v_\mathrm{r})\frac{\mu_0}{1+\mu_0}\right)(c_1(\mathrm{abs}(v_\mathrm{r})-1)^2+1)H(h), \tag{3.6}$$

where μ_0 is a static friction coefficient.

Motion of the analysed system can be described by a set of two second-order differential equations, which is presented here in a non-dimensional form,

$$x'' + 2\xi_x x' + x = f_x(y, x', y'), \tag{3.7}$$

$$y'' + 2\xi_y\sqrt{\alpha}y' + \alpha y = f_y(y, x', y'), \tag{3.8}$$

where

$$\xi_x = \frac{k_x}{2m\omega_{0x}}, \qquad \xi_y = \frac{k_y}{2m\omega_{0y}}, \qquad \alpha = \frac{c_y}{c_x}, \qquad \omega_{0x}^2 = \frac{c_x}{m}, \qquad \omega_{0y}^2 = \frac{c_y}{m}.$$

Equations (3.7) and (3.8) are transformed into a system of four first-order differential equations, which can be written as follows,

$$\left.\begin{aligned} x_1' &= x_2, \\ x_2' &= -x_1 - 2\xi_x x_2 + f_{x2}(x_2, x_3, x_4), \\ x_3' &= x_4, \\ x_4' &= -\alpha x_3 - 2\xi_y\sqrt{\alpha}x_4 + f_{x4}(x_2, x_3, x_4), \end{aligned}\right\} \tag{3.9}$$

where

$$f_{x2}(x_2, x_3, x_4) = f_x(y, x', y'), \tag{3.10}$$

$$f_{y2}(x_2, x_3, x_4) = f_y(y, x', y'). \tag{3.11}$$

To solve (3.9), the corresponding initial condition was specified, $\boldsymbol{x} = \mathbf{0}$, where $\boldsymbol{x} = [x_1, x_2, x_3, x_4]^\mathrm{T}$. The expressions for the cutting forces (3.4) and (3.6) have five different discontinuities, which can be classified into one of two groups: either to the 'continuous' discontinuity (non-smooth function), *DiscC*; or 'discontinuous' discontinuity, *DiscD*. This classification was used to design a precise integration scheme, which is based on the fourth-order Runge–Kutta algorithm. The discontinuity *DiscC*

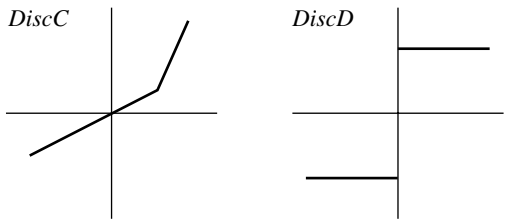

Figure 3. Discontinuity type *DiscC* and *DiscD*.

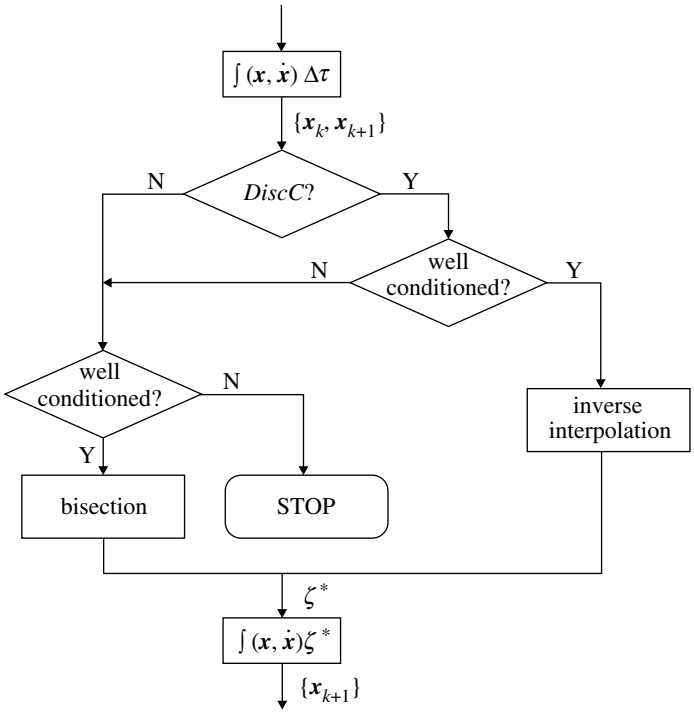

Figure 4. A flowchart of finding the time of discontinuity.

is a product of a linear and a Heaviside function, whereas *DiscD* is a straightforward signum function (see figure 3*b*).

As the analysed system is nonlinear and can exhibit a broad range of responses, it is essential to provide a high-accuracy integration routine. Each time a discontinuity occurs, the precise value of the time has to be calculated in order to provide the correct initial conditions for the next integration step. A standard zero-finder algorithm cannot effectively be applied in this case, therefore the computations were conducted using the method specifically developed for this problem, for which a flowchart is presented in figure 4, and will be discussed briefly below. For a given set of parameters and initial conditions, the numerical integration is carried out using the fourth-order Runge–Kutta procedure with a fixed time-step, $\Delta\tau = 0.001$, until a discontinuity is detected. Then, based on the type of discontinuity recognized, the precise time value, ξ^*, is calculated, either by an inverse interpolation or a bisection routine.

Dynamic responses of the system may be portrayed by a family of the characteristics depicted in figure 5, where the system non-periodicity in both directions,

x (parts (a) and (b)) and y (parts (e) and (f)), is confirmed by the phase plane portraits (parts (c) and (g)). The intermittency of the cutting-force components (parts (d) and (h)) coincides with an erratic profile of the surface (part (i)).

The investigated system is described by a 12-parameter vector,

$$\boldsymbol{p} = [\alpha, \xi_x, \xi_y, \mu_0, c_1, c_2, c_3, c_4, q_0, h_0, R_0, v_0]^{\mathrm{T}}.$$

However, for the purpose of this analysis, a two-parameter vector, $\boldsymbol{p}^* = [\xi, q_0]^{\mathrm{T}}$, was chosen, where $\xi_x = \xi_y = \xi$. The results presented here were obtained by fixing the values of the following parameters, i.e. $\mu_0 = 0.1$, $c_1 = 0.3$, $c_2 = 0.7$, $c_3 = 1.5$, $c_4 = 1.2$, $h_0 = 0.5$, $R_0 = 2.2$ and $v_0 = 0.5$. Figures 6 and 4 show an influence of the cutting force modules, q_0, on the system dynamics in the x- and y-direction, respectively.

For the stiffness ratio, α, equal to 0.25, and q_0 up to 1.6, the system behaves in a irregular manner. By increasing the value of q_0 above 1.6, the periodicity is regained. Further careful investigations of the above-mentioned region of q_0 demonstrate an interesting scenario of a transition between different types of motion with an increase of the branching-parameter value. The system responses are irregular for lower values of q_0, however, irregularities are more pronounced for the y-direction. If a value of the branching parameter is between 0.36 and 0.43, the system experiences period 3. After the first periodic region, a catastrophic transition to a chaotic motion is observed, which lasts until $q_0 \approx 1.0$. Then the system approaches gradually stable oscillations, with period 1 passing through narrow *windows of irregular motion*. Summarizing, for $\alpha = 0.25$, the system dynamics undergoes vast changes. Setting up the stiffness ratio, α, to 1 and 16, the behaviour is completely different (see figures $6b, d$ and $7b, d$). For almost the entire range of the cutting-force modulus, the system oscillates either periodically or almost periodically, excluding the lower values of q_0, where some transient irregular motion occurs. The bifurcation diagrams constructed for $\alpha = 4$ show another example of an unusual behaviour, that is, unidirectional bifurcation. The system bifurcates in the x-direction and is stable in the y-direction, for q_0 between 0.24 and 0.54, despite the fact that the equations of motion are coupled. There is also a shift of the critical point for the x- and y-directions. For the x-direction, the system starts with two bifurcation periods of the doubling type, and then vibrates chaotically. For the y-direction, the system, after crossing the critical value, oscillates with period 4, and then becomes chaotic. The bifurcation diagrams depicted in figure 6 show that, for $\alpha = 0.25$ and $\alpha = 1.0$, the system, after regaining periodicity, decreases its vibration amplitude with an increase of the cutting force. This fact can be used in the design of the machine tools and control of the cutting processes. For $\alpha = 16$, the system responses are consistent with a traditional understanding of the MT–CP interactions, i.e. higher amplitudes are generated by larger cutting forces. For this simple orthogonal cutting process, dimensional accuracy can be viewed through the displacement in the y-direction alone. The calculated results depicted in figure 7 indicate that the most favourable cutting conditions can be obtained for the stiffness ratio α equal to 1.

Now, through the construction of bifurcation diagrams x, $y = f(\xi)$, we examine the influence of the viscous damping coefficient, ξ, on the displacements in the x- and y-directions. As shown in figure 8, for ξ smaller than 0.26, the results coincide with the linear vibration theory prediction, i.e. a higher damping ratio stabilizes the system responses. When this critical value is passed, the system vibrates periodically in both the x- and y-directions, until a fascinating phenomenon is detected, i.e. *the*

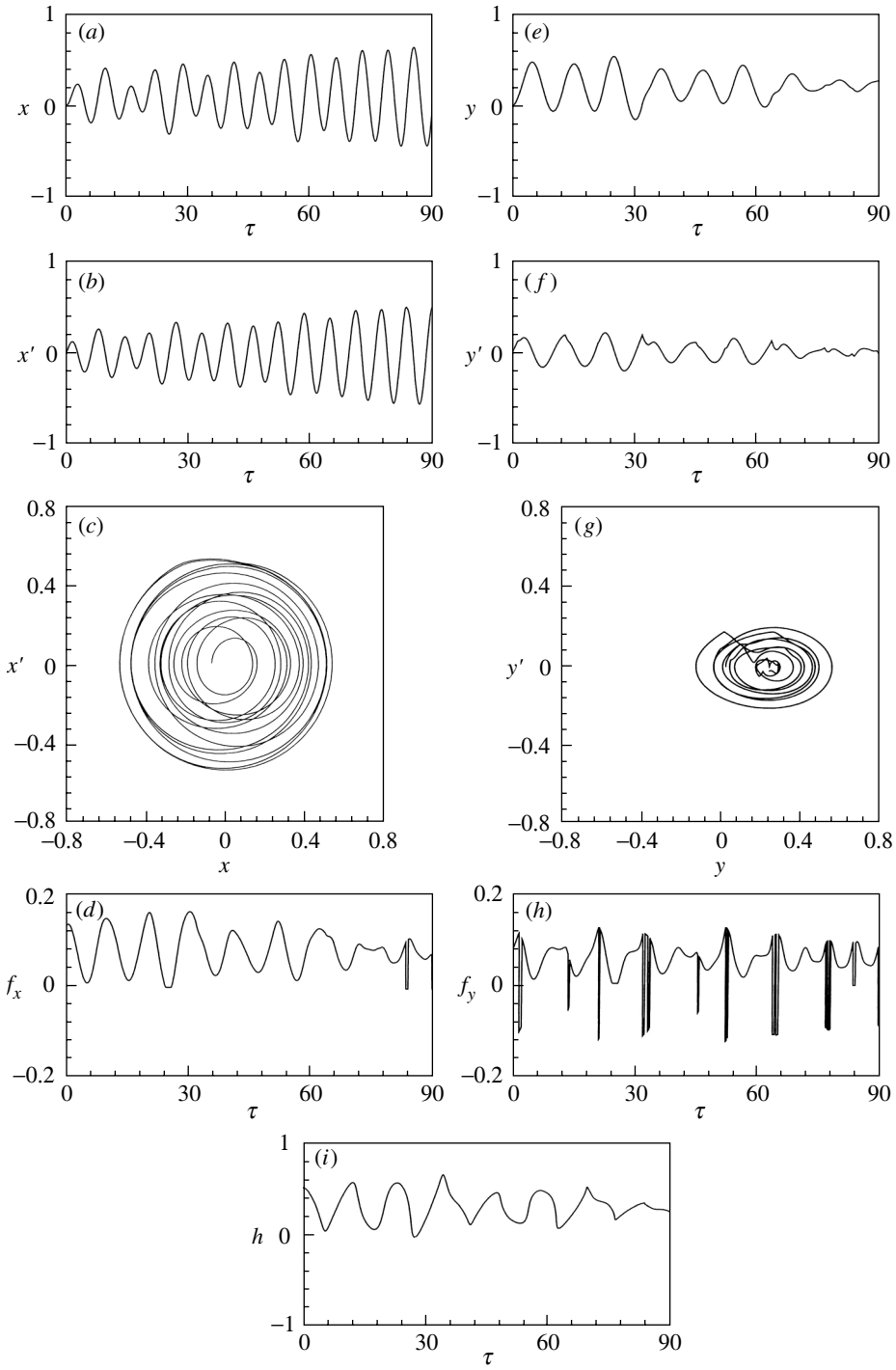

Figure 5. A family of characteristics for the MT–CP system.

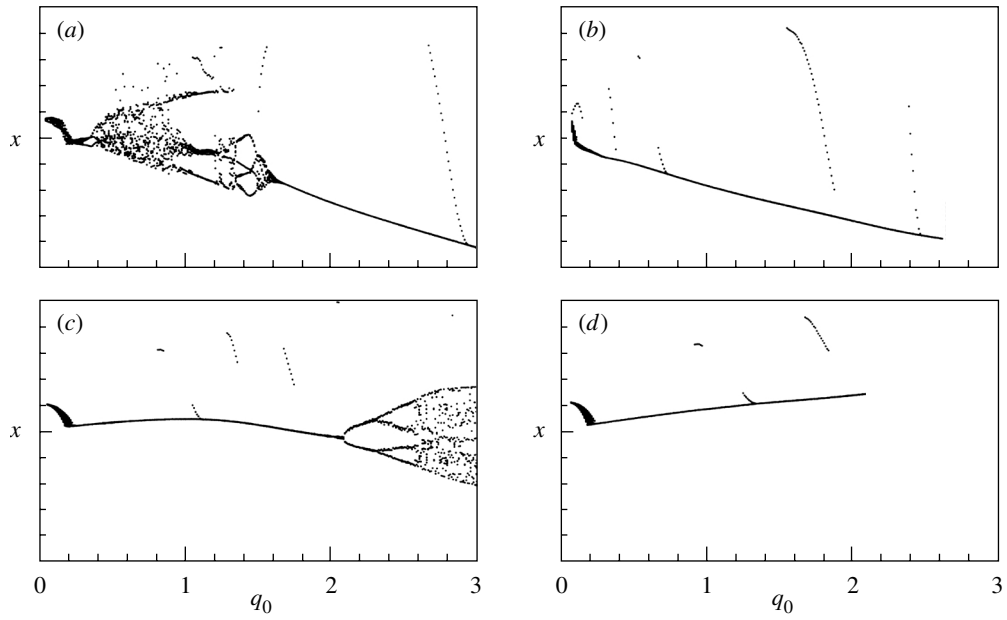

Figure 6. Bifurcation diagrams $x = f(q_0)$. (*a*) $\alpha = 0.25$. (*b*) $\alpha = 1$. (*c*) $\alpha = 4$. (*d*) $\alpha = 16$.

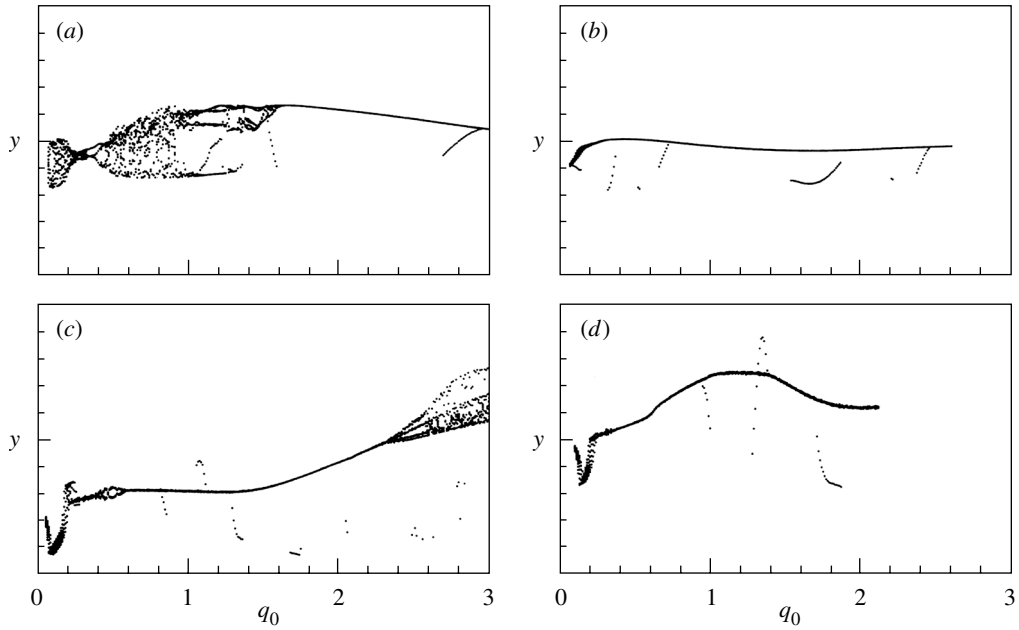

Figure 7. Bifurcation diagrams $\alpha = f(q_0)$. (*a*) $\alpha = 0.25$. (*b*) $\alpha = 1$. (*c*) $\alpha = 4$. (*d*) $\alpha = 16$.

deaths and births of periodic solutions, as the damping ratio increases. This can be understood as follows: the system is asymptotically stable in the finite intervals, and oscillates periodically for a finite number of discrete values of the branching parameter. This curiosity occurs for both directions.

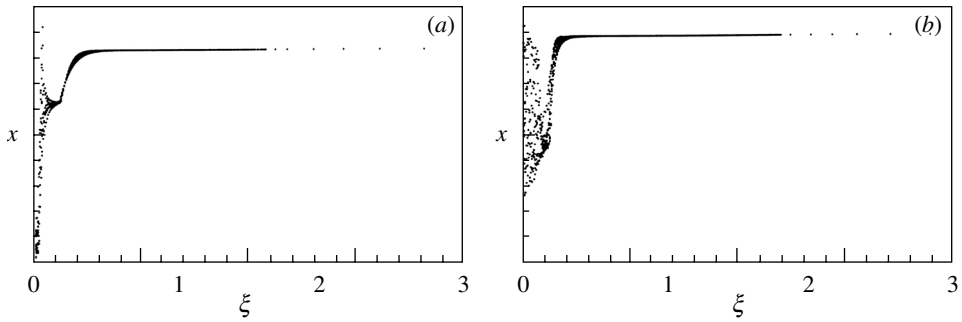

Figure 8. Bifurcation diagrams. (*a*) $x = f(\xi)$, (*b*) $y = f(\xi)$.

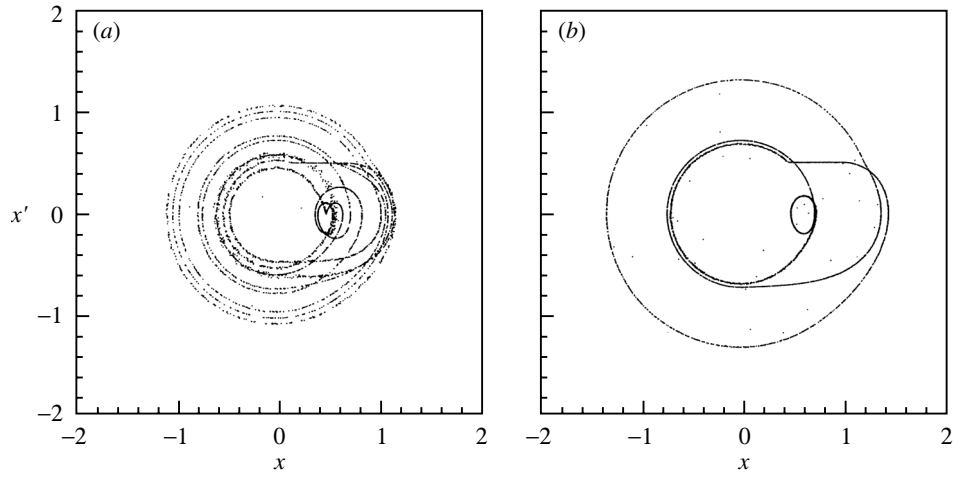

Figure 9. Poincaré map $x_{n+1} = f(x_n)$ for (*a*) $q_0 = 1.0$ and (*b*) $q_0 = 1.25$.

Any categorical statement about the existence of chaos in the system requires a consistency between the proofs obtained from different quality of motion-detecting techniques. Constructing Poincaré maps is helpful to assess and classify the dynamic system responses for two different values of the branching parameter, e.g. module of the cutting force q_0. For instance, considering two cross-sections of the bifurcation diagram depicted in figure 6 at $q_0 = 1.0$ and $q_0 = 1.25$, the chaotic motion is forecast for the first case. Nevertheless, the system responses are revealed to be subharmonic for both values of the branching parameter. The suspected chaotic motion for $q_0 = 1.0$ is, in fact, period 11, and the other one is period 4. However, one can recognize some signs of chaotic motion from the presented Poincaré sections, i.e. the periodic orbits are accompanied by 'clouds' of irregular points. This may be explained by the existence of transient chaotic motion, which usually dies out in the long term.

As far as the dynamics of the cutting process is concerned, it would be interesting and beneficial to observe trajectories of the cutting edge for the above-analysed cases of different forms of motion. Moreover, it would help to view the obtained results through different hypotheses of the self-excited vibration. As the analysed system can produce complex behaviour (including chaotic), and for the practical reason outlined above, one constructs Poincaré maps of the trajectories instead of the trajectories themselves. This is more convenient in most cases, as a replacement of a trajectory

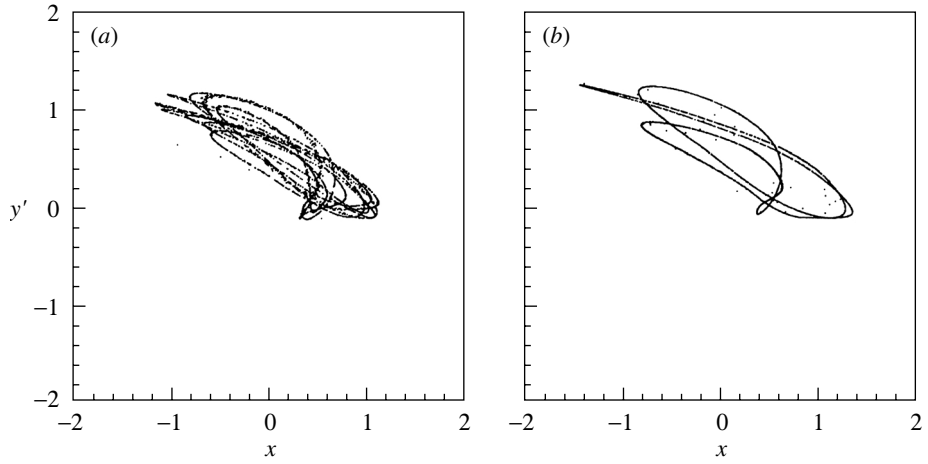

Figure 10. Poincaré map of the cutting edge trajectory for (*a*) $q_0 = 1.0$ and (*b*) $q_0 = 1.25$.

by its Poincaré section can simplify the process of the system response recognition. Figure 10 shows two topologies of the Poincaré maps obtained for the same values of those parameters used in figure 9. The presented maps do not correlate fully with any of the self-excited vibration hypothesis; however, some similarities with the falling friction force hypothesis can be recognized from figure 10.

(*b*) *Stochastic model*

As has been mentioned earlier, though considerable progress in the modelling of dynamic interactions occurring during metal cutting has been made, the models are mostly deterministic, using average values of the cutting-material coefficients, and do not take into account the stochastic issues. In particular, because of the varying grain size of the workpiece, the randomness of the cutting resistance is worth examining. Chip irregularities are influenced by an inhomogeneity of the material being cut, which leads to a random cutting resistance. A rigorous mathematical treatment of the plastic deformation for inhomogeneous material is a complex issue and so far no solid foundation has been laid in this area. As a consequence, a simple but pragmatic approach is used to model the cutting resistance. This can be expressed as a function of the cutting-tool trajectory (Wiercigroch & Cheng 1997),

$$c(\boldsymbol{r}) = c(x, y, z), \tag{3.12}$$

where $\boldsymbol{r}(t) = (x(t), y(t), z(t))$ is a parametric function of time. It is postulated that the material inhomogeneity is a stationary Gaussian process. Hence it is reasonable to assume that the variation of the cutting resistance is also a stationary Gaussian process. In general, this process is three dimensional. However, in this paper we consider the cutting resistance as a one-dimensional process, which is a reasonable approximation for orthogonal cutting. It is assumed that the cutting resistance has been normalized by its mean, hence the mean value is equal to 1,

$$\bar{c} = \lim_{l\to\infty} \frac{1}{l} \int_0^l c(x)\,\mathrm{d}x = 1, \tag{3.13}$$

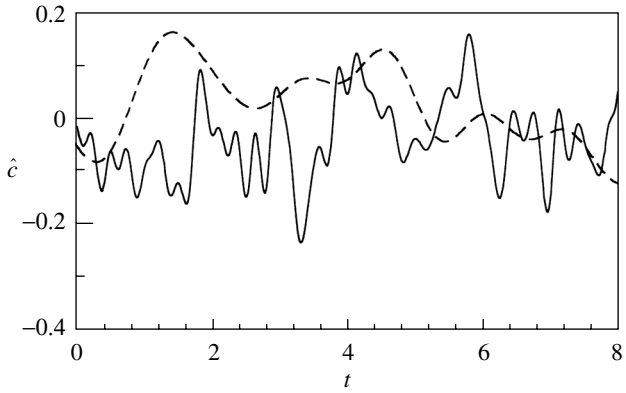

Figure 11. Stochastic specific cutting resistance for $\lambda = 1$ (dashed line) and $\lambda = 5$ (solid line).

where l is a reference length of cut, and $c(x)$ is the normalized specific cutting resistance. Subtracting the mean value from $c(x)$, we obtain the fluctuation quantity $\hat{c}(x) = c(x) - \bar{c}$, where $\hat{c}$ is a zero-mean one-dimensional univariate weakly stationary Gaussian process. It is characterized by a standard deviation σ, and an autocorrelation coefficient $R(z)$, where z is the distance separating two points. A power spectral density function $S(\omega)$ is defined as

$$S(\omega) = \frac{1}{2\pi} \int_{-\infty}^{\infty} R(z) \mathrm{e}^{-\omega x} \, \mathrm{d}z. \tag{3.14}$$

The autocorrelation coefficient is typically characterized by a correlation length, which is related to the distance beyond which the correlation of the material fluctuation diminishes. The correlation length and the form of the autocorrelation function should be determined experimentally, either by a direct testing of the material or by an interpretation of the vibration signal. Unfortunately, to our knowledge, no such measurements are available. From the material-science point of view, the correlation length should be mainly dependent upon the grain size of the material, hence an estimate can be made. As a first-cut approximation, a simple but popular model for the autocorrelation coefficient is adopted for the present study,

$$R(z) = \mathrm{e}^{-\lambda |z|}. \tag{3.15}$$

In the above, $1/\lambda$ characterizes the correlation length. The power spectral density function corresponding to (3.14) is

$$S(\omega) = \frac{\lambda}{\pi(\lambda^2 + \omega^2)}. \tag{3.16}$$

With the above statistical quantities, it is possible to generate a stochastic signal with the same statistics. The technique adopted is the spectral representation method initiated by Rice (1954) and refined by Shinozuka & Jan (1972) and Shinozuka & Deodatis (1992). It is modelled by the following series,

$$\hat{c}(x) = 2\sigma \sum_{k=0}^{N-1} \sqrt{S(\omega_k) \Delta\omega \cos(\omega_k x + \phi_k)}, \tag{3.17}$$

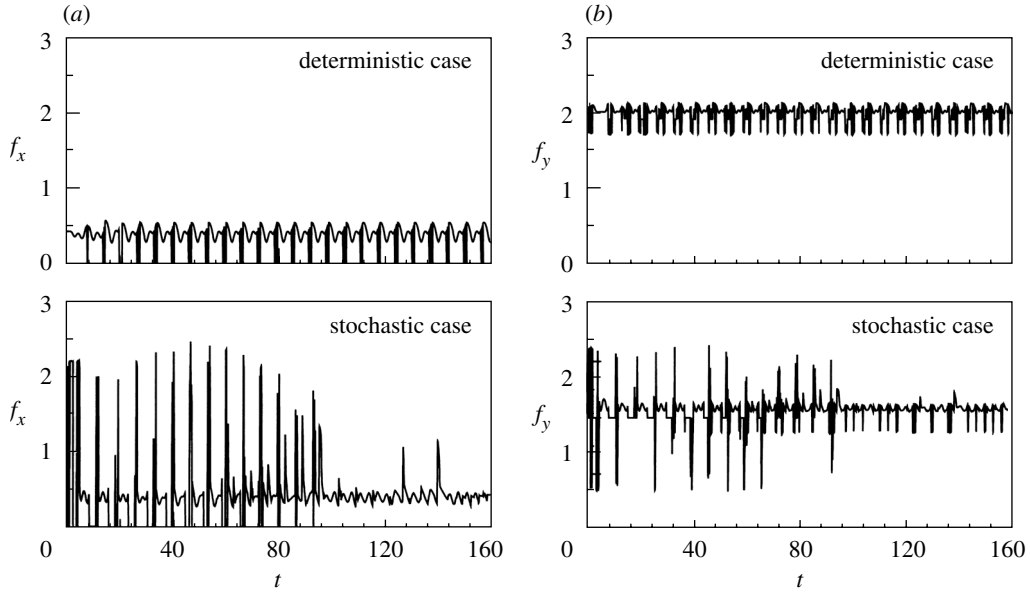

Figure 12. Time-histories for the (a) x-component and (b) y-component of the cutting force.

where σ is the standard deviation, ϕ_k is a random phase angle uniformly distributed over $[0, 2\pi]$, $\omega_k = k\Delta\omega$, and $\Delta\omega$ is the frequency increment. The process (3.17) has been simulated, and two different realizations of $\hat{c}(x)$ are depicted in figure 11. The calculations were carried out for the same standard deviation ($\sigma = 0.2$), but for different λ values, 1 and 5. It can be noted that as λ gets larger, the correlation length becomes smaller, and the data fluctuate more rapidly.

Assuming the same mathematical model of the MT–CP system as in the previous section, the cutting forces f_x and f_y depend upon the stochastic properties of the workpiece, which are modelled by the randomness of the specific cutting resistance $c(x)$,

$$f_x(x, y, x', y') = c(x)q_0 hH(v_\mathrm{r})(c_1(v_\mathrm{r} - 1)^2 + 1)H(h). \tag{3.18}$$

The most dangerous state for a cutting tool is the transient period when a new layer is being cut. Impacts between the tool and the workpiece occur frequently; therefore, it would be beneficial to predict the time-histories of the cutting forces. Investigations have been carried out for the deterministic model. No substantial increase in the cutting forces was reported. This is, however, not the case once the stochastic cutting resistance is modelled. To demonstrate this effect, parts (a) and (b) of figure 12 compare the time-histories of the cutting forces f_x and f_y, for the deterministic (constant cutting resistance) and the stochastic (randomly fluctuating cutting resistance) cases. For the stochastic model, $\sigma = 0.2$ and $\lambda = 1$ are used. For the deterministic case (upper diagrams), we note that the transient period is relatively short, and that there is no abnormal response during that period. These confirm the earlier findings. The x-component cutting force exhibits discontinuities that correspond to the loss of contact between the tool and the workpiece. The stochastic results are shown as the lower diagrams of parts (a) and (b) of figure 12. We observe not only a longer transient period, but also a much greater impact force. In the x-direction, where the tool undergoes a higher stress, the force

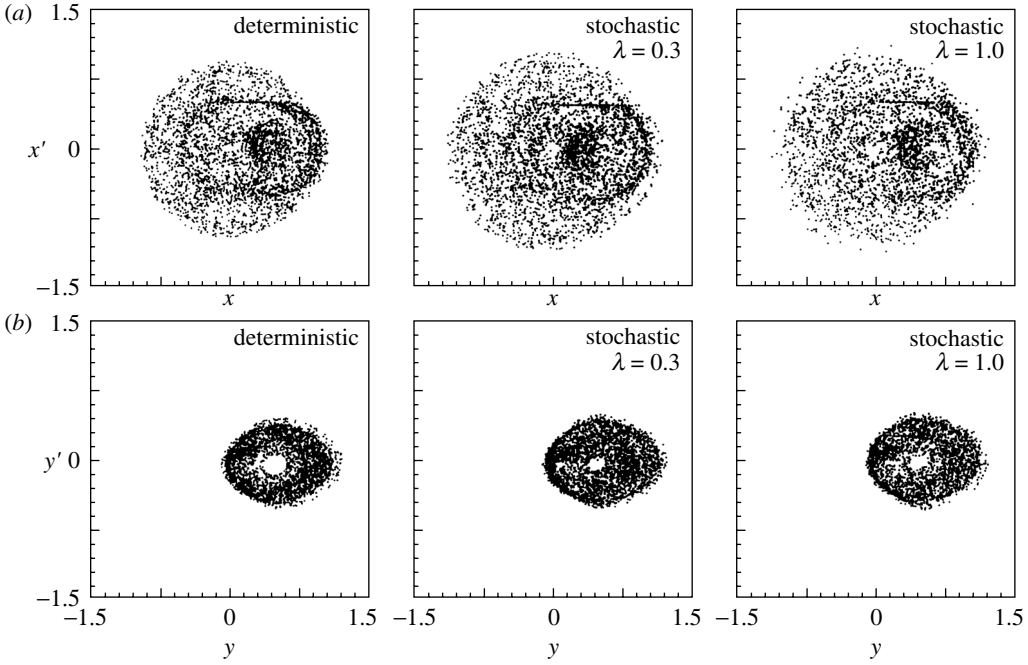

Figure 13. Poincaré maps in the (a) (x, x')-plane and (b) (y, y')-plane for deterministic and stochastic cases, with different values of λ.

can be as much as 300% greater than the average value under steady cutting conditions. The time-interval of tool separation is also longer. This current theoretical prediction, which was not reported before, is consistent with the manufacturing reality, i.e. the majority of cutting-tool breakages occur during the transient period. To get the overall picture, the long-term dynamic behaviour needs to be addressed.

The Poincaré maps are used to examine a long trend, hence the initial transient period is skipped. Parts (a) and (b) of figure 13 display the Poincaré points (x, x') and (y, y'), respectively.

Both the deterministic and the stochastic cases are shown. For the stochastic case, two λ values, 1.0 and 0.3, are used, where $1/\lambda$ corresponds to the correlation length. The deterministic case may be viewed as the case $\lambda \to 0$, i.e. the data are fully correlated. Reading the figures from the top down, the correlation length decreases, meaning that the rate of fluctuation of cutting resistance increases. For all cases, we observe that the responses are chaotic. The stochasticity does not significantly change the topology of the Poincaré maps. Closer examination shows that the introduction of stochasticity spreads out the Poincaré maps over a slightly larger area. The concentration of points in the map is also changed. This can be more precisely assessed by the measure of a probability density function (PDF), as outlined in Yang *et al*. (1991).

The PDF samples the entire trajectory, rather than the specific Poincaré section. This technique presents the relative frequency of each region in the phase plane visited by the trajectory. The joint PDF is determined by overlaying a grid system on the phase plane. By counting the number of points falling within each grid and nor-

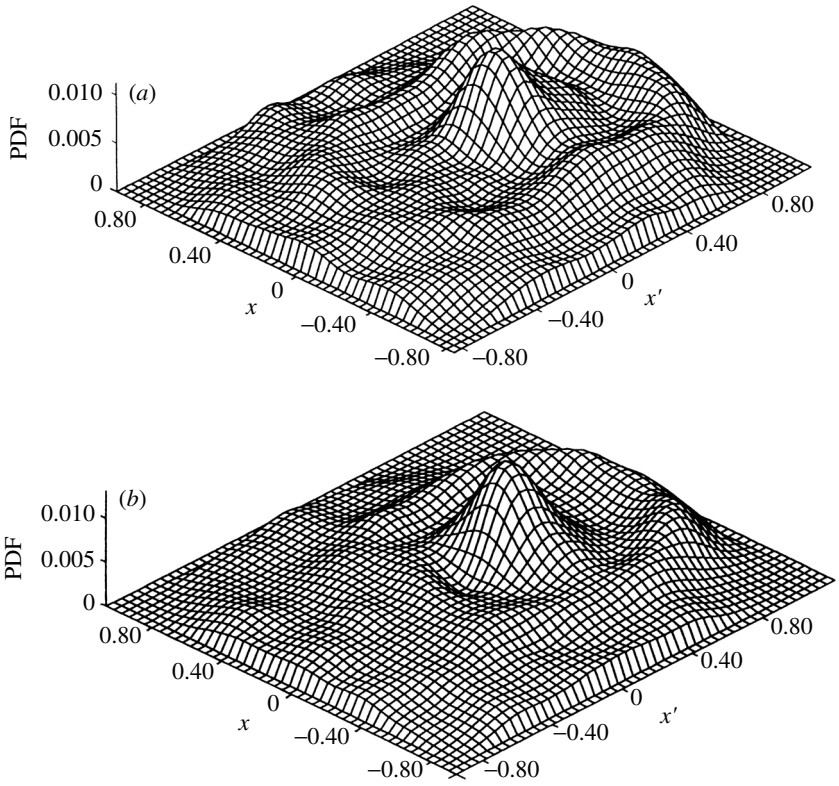

Figure 14. Joint probability density function for the (*a*) deterministic and (*b*) stochastic ($\lambda = 0.3$) case.

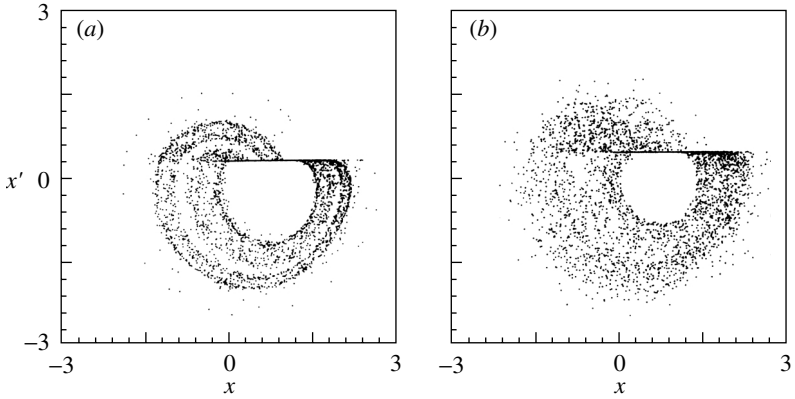

Figure 15. Poincaré maps of pseudo-stochastic process constructed for a reference length of (*a*) $\underline{x} = 20$ and (*b*) $\underline{x} = 100$.

malizing, the joint PDF is produced. The result for the (x, x') phase plane is depicted in figure 14, for the deterministic and the stochastic ($\lambda = 0.3$) case, respectively. A comparison of the two PDFs shows that the randomness of cutting resistance tends to smooth out some fine features of the deterministic case.

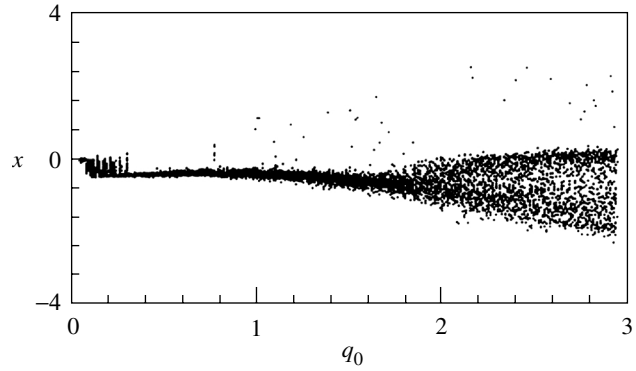

Figure 16. Stochastic bifurcation diagram as a function of modulus of the cutting force.

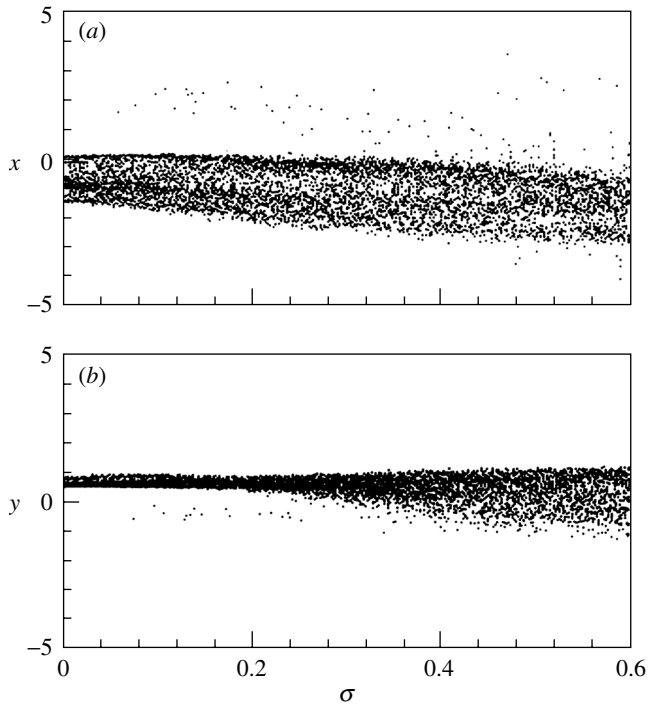

Figure 17. Bifurcation diagrams as a function of the standard deviation for the (*a*) *x*- and (*b*) *y*-direction.

The long time-histories required to construct Poincaré maps make the task computationally intensive. For the stochastic case, it is necessary to construct the stochastic cutting resistance data that cover the whole period of simulation, which often involves several thousand cycles. The computation time for generating these data can be one to two orders of magnitude larger than an average time spent for the deterministic system. This is particularly so for cases with a shorter correlation length (larger λ). Therefore, in order to reduce the computing time, a pseudo-stochastic process was used, as shown in figure 15.

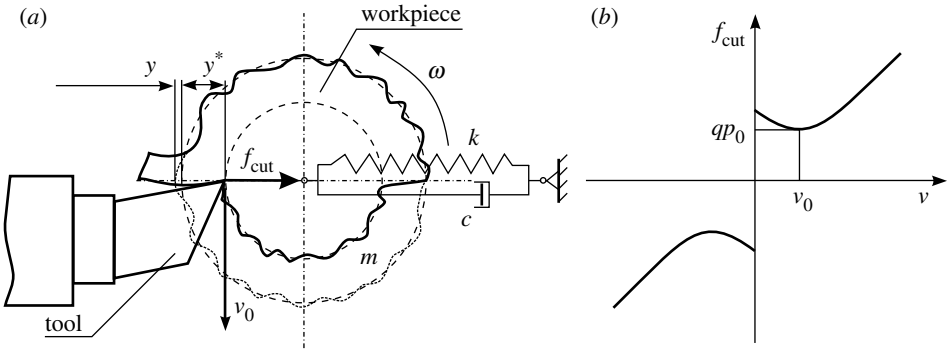

Figure 18. (*a*) Physical model; (*b*) dry friction characteristics.

So far, the differences in system response for the deterministic and the stochastic cases, under a fixed set of system parameters, have been examined. To scan the effect for a whole range of parameters, bifurcation diagrams were constructed. Figure 16 presents a bifurcation diagram, where x is a function of the cutting-force magnitude, q_0. Figure 16 shows a bifurcation diagram obtained for $\lambda = 1$ and $\sigma = 0.2$, using the same parameters as in figure 6*c*. The comparison with the deterministic case shows that the stochasticity not only smears the amplitude of vibration, but also moves the first critical point of the first period doubling to a lower value. It also destroys the second period doubling. In some other cases, which are not shown here, it is impossible to distinguish any critical point on the bifurcation diagram.

The study carried out by Kapitaniak (1990) shows that the introduction of a random noise to nonlinear continuous systems exhibiting chaotic behaviour (say, a Duffing oscillator) can drastically decrease its chaoticity. Its influence on a discontinuous system, such as the one investigated here, is unknown. In figure 17, a bifurcation diagram is constructed by choosing the standard deviation as a branching parameter. It should be noted that the deterministic system ($\sigma = 0$) is chaotic. Even a substantial increase in the magnitude of noise does not dampen the chaoticity of the system. On the contrary, random noise tends to increase the system irregularity, especially in the y-direction.

4. Stability analysis

In order to keep the analysis clear, we will consider stability of the one-degree-of-freedom model of the cutting process (figure 18*a*), with the dry friction shown in figure 18*b*. Similar to the two-degree-of-freedom model discussed in Wiercigroch (1997), the dry friction force between the tool and the workpiece is assumed to be as depicted in figure 18*b*. This relation can be expressed by the following formula,

$$f_{\mathrm{cut}} = q[p_0 + \gamma(v_0 - |v|)^2] \operatorname{sgn} v, \tag{4.1}$$

where q is a depth of cut function, p_0 is a constant related to minimum friction force, v_0 is a prescribed velocity, and γ represents a degree of nonlinearity.

The depth of cut function is calculated as

$$q = q_0(y_* - y)\mathcal{H}(y_* - y), \qquad v = v_* - \dot{y}, \tag{4.2}$$

where y_* is a depth of cut, v_* is an average relative velocity between the tool and the workpiece, $\mathcal{H}$ is the Heaviside function. Substitution of (4.2) into (4.1) gives

$$f_{\rm cut} = q_0(y_* - y)\mathcal{H}(y_* - y)[p_0 + \gamma(v_0 - |v_* - \dot{y}|)^2]\,\mathrm{sgn}(v_* - \dot{y}). \tag{4.3}$$

If the vibrations in a vicinity of the stationary point $y = 0$, $\dot{y} = 0$ are not very intensive, then conditions $\dot{y} < v_*$ and $y < y_*$ are satisfied, and formula (4.3) is reduced to the following form:

$$f_{\rm cut} = q_0(y_* - y)[p_0 + \gamma(u + \dot{y})^2], \qquad u \stackrel{\rm def}{=} v_0 - v_*. \tag{4.4}$$

The relative motion between the tool and the workpiece is described by the following equation,

$$m\ddot{y} + c\dot{y} + ky = f_{\rm cut}, \tag{4.5}$$

where m is the mass of the workpiece, c is the viscous friction coefficient, k is the equivalent stiffness, and $f_{\rm cut}$ is the cutting force. Dividing (4.5) by m and substituting formula (4.4) for the cutting force, one can obtain

$$\ddot{y} + 2\eta\dot{y} + \omega^2 y = c_0(y_* - y)[p_0 + \gamma(u + \dot{y})^2], \tag{4.6}$$

where

$$\eta \stackrel{\rm def}{=} \frac{c}{2m}, \qquad \omega^2 \stackrel{\rm def}{=} \frac{k}{m}, \qquad c_0 \stackrel{\rm def}{=} \frac{q_0}{m}.$$

Without losing generality of the approach, we can assume $c_0 \equiv 1$. After some transformations the above equation can be represented as

$$\ddot{y} + \alpha(y, \dot{y})\dot{y} + \omega_1^2 y = \omega_1^2 y_1, \tag{4.7}$$

where

$$\alpha(y, \dot{y}) \stackrel{\rm def}{=} 2\eta - \gamma(y_* - y)(2u + \dot{y}) = 2\eta_1 + \gamma(2uy - y_*\dot{y} + y\dot{y}),$$

$$\eta_1 \stackrel{\rm def}{=} \eta - \gamma u y_*, \qquad \omega_1^2 \stackrel{\rm def}{=} \omega^2 + p_0 + \gamma u^2, \qquad \omega_1^2 y_1 \stackrel{\rm def}{=} (p_0 + \gamma u^2)y_* = (\omega_1^2 - \omega^2)y_*.$$

It is worth noting that the natural frequency of the system changes due to the nonlinear friction force; the new natural frequency is always greater then the original, $\omega_1 > \omega$. In addition, the nonlinear friction has shifted the equilibrium position to $y = y_1$, where $0 < y_1 < y_*$. By changing variables $z = y - y_1$ the equilibrium returns to the zero position and equation (4.7) reduces to

$$\ddot{z} + \beta(z, \dot{z})\dot{z} + \omega_1^2 z = 0, \tag{4.8}$$

where

$$\beta(z, \dot{z}) \stackrel{\rm def}{=} 2\eta - \gamma(z_* - z)(2u + \dot{z}) = 2\eta_2 + \gamma(2uz - z_*\dot{z} + z\dot{z}),$$

$$z_* = y_* - y_1 = (\omega^2/\omega_1^2)y_*, \qquad \eta_2 \stackrel{\rm def}{=} \eta - \gamma u z_*, \qquad \omega_1^2 \stackrel{\rm def}{=} \omega^2 + p_0 + \gamma u^2.$$

Note that since $y < y_*$, it holds that $z < z_*$.

Consider now equation (4.8), where the value of the nonlinear dissipation coefficient $\beta(z, \dot{z})$ in the equilibrium, $z = 0$, $\dot{z} = 0$, is

$$\beta(0, 0) = 2\eta_2, \qquad \eta_2 = \eta - \gamma u z_*, \qquad u = v_0 - v_*, \qquad z_* = (\omega^2/\omega_1^2)y_*. \tag{4.9}$$

The above coefficients η, γ, z_* are positive and only the sign of the coefficient u can change. If $\beta(0,0) > 0$, then the equilibrium will be stable and no chatter can appear. From (4.9) it follows that negative value of the coefficient u is the necessary condition for the stability, which yields the following conclusion. *If the optimum velocity v_0 for the dry friction force is smaller than the average relative velocity v_* between the tool and the workpiece, $v_0 < v_*$, then the cutting process is stable.* The necessary and sufficient condition of stability is $\eta_2 = \eta - \gamma u z_* > 0$. For the case of relatively small friction it holds that $z_* \approx y_*$, which gives the following stability condition:

$$v_0 < v_* + \frac{\eta}{\gamma y_*}. \tag{4.10}$$

From the above inequality it follows that an increase of the depth of cut y_* and the dry friction nonlinearity γ decrease the stability.

For a higher friction the frequency z_* itself is a function of $u = v_0 - v_*$, hence the condition $\eta_2 > 0$ leads to the following quadratic inequality with respect to u:

$$\eta\gamma u^2 - \gamma\omega^2 y_* u + \eta(\omega^2 + p_0) > 0. \tag{4.11}$$

The determinant, D, of the above quadratic polynomial is equal to

$$D = (\gamma\omega^2 y_*)^2 - 4\eta^2\gamma(\omega^2 + p_0). \tag{4.12}$$

From the above formula it follows that for large enough viscous damping η, D is negative and inequality (4.11) will be satisfied for any velocities v_0, v_*. Therefore, a large viscous friction can always prevent chatter. After solving the quadratic equation, inequality (4.11) yields the following stability conditions,

$$v_0 < v_* + u_1 \quad \text{or} \quad v_0 > v_* + u_2, \tag{4.13}$$

where

$$u_1 \stackrel{\text{def}}{=} \frac{\gamma\omega^2 y_* - \sqrt{D}}{2\eta\gamma}, \qquad u_2 \stackrel{\text{def}}{=} \frac{\gamma\omega^2 y_* + \sqrt{D}}{2\eta\gamma}.$$

Consider now the nonlinear coefficient of dissipation $\beta(z, \dot{z})$. For $\beta(0,0) < 0$ the equilibrium is unstable. Chatter appears when a limit cycle is formed, which is possible if the coefficient $\beta(z, \dot{z})$ changes sign for larger amplitudes. Therefore, consider now a condition $\beta(z, \dot{z}) = 0$, which gives

$$\gamma(z_* - z)(2u + \dot{z}) = 2\eta. \tag{4.14}$$

The solution of the above equation in the phase plane z, $\dot{z}$ is a hyperbole with asymptotes $z = z_*$ and $\dot{z} = -2u$. Remember that $z < z_*$, so the asymptote $z = z_*$ gives the boundary for the area of the admissible z values. On the asymptote the function $\beta(z, \dot{z})$ has a positive value of 2η. Thus the dissipation-of-energy coefficient changes its sign in the admissible area, which confirms a possibility of the chatter occurrence.

The problem of the self-excited vibration can be effectively investigated from the energy balance point of view. Multiplying equation (4.8) by $\dot{z}$ allows us to transform it to the energy-based,

$$\dot{\mathcal{E}} = -\beta(z, \dot{z})\dot{z}^2, \qquad \mathcal{E} \stackrel{\text{def}}{=} \tfrac{1}{2}(\dot{z}^2 + \omega_1^2 z^2), \tag{4.15}$$

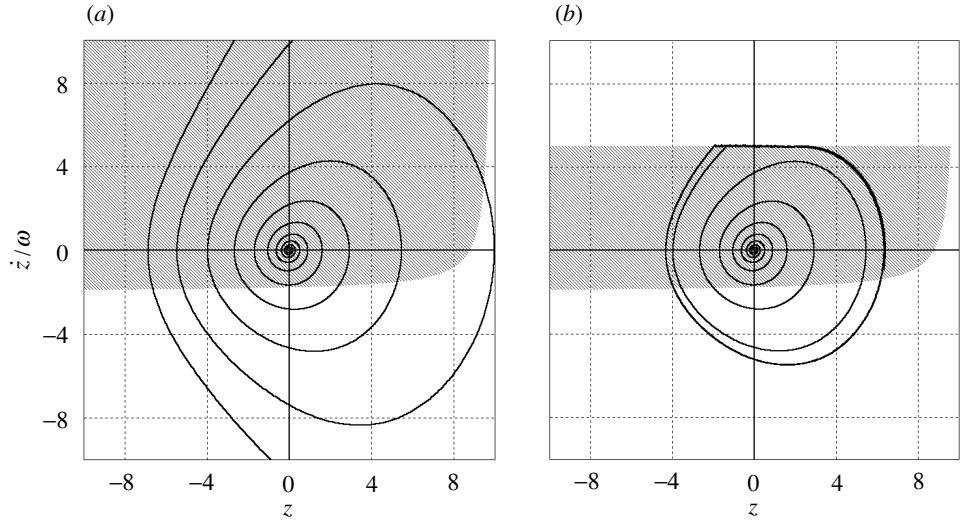

Figure 19. Phase plane for (*a*) continuous dissipation force, (*b*) discontinuous dissipation force.

where $\mathcal{E}$ is a quantity proportional to the mechanical energy of the system. If T is the period of the chatter, then on the limit cycle of the chatter the condition $\mathcal{E}(t+T)-\mathcal{E}(t)\equiv 0$ should be fulfilled. Let us define

$$J \stackrel{\text{def}}{=} \int_0^T \beta(z,\dot{z})\dot{z}^2\,\mathrm{d}t = \mathcal{E}(T)-\mathcal{E}(0). \tag{4.16}$$

Note that $J\equiv 0$ on the limit cycle of the chatter oscillations. If the dry friction force is small, then the oscillations should not differ much from harmonic oscillations. Therefore, let us approximate $z(t)$ in the above equation by a harmonic function $z(t)=A\sin\omega_1 t$. Then the above integral takes the form,

$$J = A^2\omega_1\int_0^{2\pi}\beta(A\sin\tau,\omega_1 A\cos\tau)\cos^2\tau\,\mathrm{d}\tau, \tag{4.17}$$

where $\tau\stackrel{\text{def}}{=}\omega_1 t$. The function $\beta(z,\dot{z})$ can be represented as

$$\beta(z,\dot{z}) = 2\eta_2 + 2\gamma u z - \gamma z_*\dot{z} + \gamma z\dot{z}.$$

A substitution of this form to (4.17) gives

$$J = A^2\omega\biggl(2\eta_2\int_0^{2\pi}\cos^2\tau\,\mathrm{d}\tau + 2\gamma uA\int_0^{2\pi}\sin\tau\cos^2\tau\,\mathrm{d}\tau - \gamma z_* A\omega_1\int_0^{2\pi}\cos^3\tau\,\mathrm{d}\tau + \gamma A^2\omega_1\int_0^{2\pi}\sin\tau\cos^3\tau\,\mathrm{d}\tau\biggr).$$

All integrals except the first are equal to zero, hence the above integral gives

$$J = 2\pi\omega_1\eta_2 A^2. \tag{4.18}$$

Thus the integral has the same sign as η_2, therefore chatter cannot be generated in the considered region $\dot{y}<v_*$, where the friction force is continuous. To confirm results

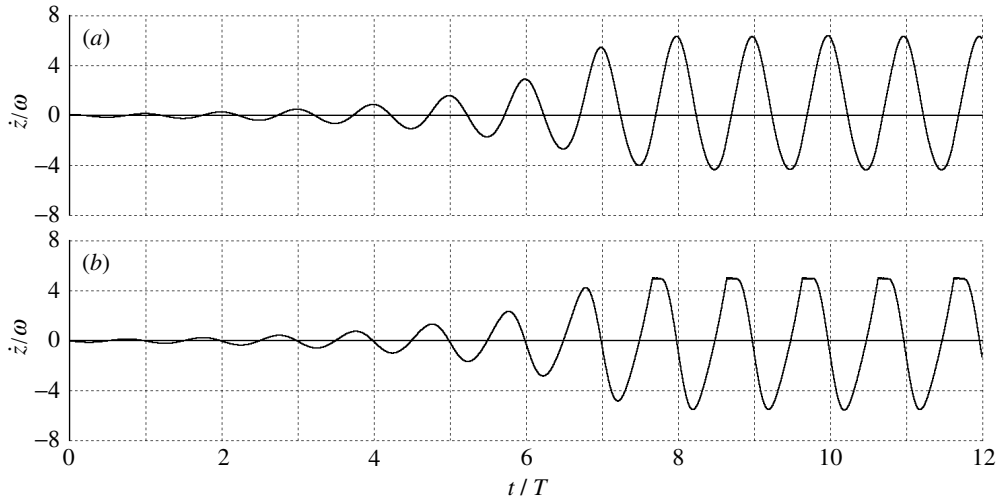

Figure 20. Time histories of the chatter appearance: (*a*) coordinate, (*b*) velocity.

just discussed, a phase plane for the equation (4.8) was computed and is depicted in figure 19*a*. Initial conditions for the phase plots are close to the position of the equilibrium. A grey tint depicts the area where the dissipative coefficient $\beta(z, \dot{z})$ is negative, and the border of this area is the hyperbola defined by equation (4.14). The picture shows that the phase curves pass the area with positive dissipation, the amplitude grows steadily. To observe chatter, a more complicated discontinuous formula (4.3) for the friction force is necessary. To simplify consideration let us assume that $y < y_*$, which practically means the tool is not leaving the workpiece. Then formula (4.3) can be rewritten in the form,

$$\frac{f}{m} = (z_* - z)[p_0 + \gamma(v_0 - |v_* - \dot{z}|)^2]\,\mathrm{sgn}(v_* - \dot{z}). \tag{4.19}$$

The phase plane calculated with the discontinuous friction force (4.19) is depicted in figure 19*b*.

The figure shows that the area with positive dissipation is extended to the zone $v > v_*$ (upper white zone in the figure). This additional dissipative zone stops the amplitude growing and forms the limit cycle, which is clearly seen in figure 19*b*. Time histories of the oscillations are presented in figure 20. The figure shows the process of the chatter generation, where the amplitude grows up from the equilibrium position and then oscillations stabilize at a certain amplitude of the chatter. On the velocity plot, flat horizontal regions can be observed, which coincide with the flat horizontal region on the phase plane figure 19*b*. In this region the tool is moving together with the workpiece, without slipping, $\dot{z} = v_*$.

Consider now energy balance equation (4.15), which in the general case can be rewritten as

$$\dot{\mathcal{E}} = N \quad \Rightarrow \quad \Delta\mathcal{E} = \int_{t=-T/2}^{T/2} N\,\mathrm{d}t, \tag{4.20}$$

where N is the power of the dissipative forces, $\Delta\mathcal{E}$ is change of the energy during one cycle (chatter period), T. On the limit cycle it holds that $\Delta\mathcal{E} = 0$ and hence

the above integral should be equal to zero. From numerical analysis it follows that if the dissipation and the coefficient of the nonlinearity γ are small enough, then the chatter period can be broken into two distinct time-intervals for $\dot{z} < v_*$ and $\dot{z} > v_*$. In each interval the dry friction function (4.19) is continuous. Assuming t_* is the length of the interval where $\dot{z} > v_*$, then for small friction the above integral on the limit cycle can be rewritten as

$$\Delta\mathcal{E} = \int_{t=t_*/2}^{T-t_*/2} N_+ \,\mathrm{d}t + \int_{t=-t_*/2}^{t_*/2} N_- \,\mathrm{d}t, \tag{4.21}$$

where N_+ and N_- are continuous parts of N, respectively, for $\dot{z} < v_*$ and $\dot{z} > v_*$. Further calculations give

$$\Delta\mathcal{E} = \int_{t=0}^{T} N_+ \,\mathrm{d}t + \int_{t=-t_*/2}^{t_*/2} (N_- - N_+) \,\mathrm{d}t, \tag{4.22}$$

where, in the second term, function N_+ is extended continuously to the interval $-t_*/2 < t < t_*/2$. As previously, let us assume $z(t) = A\sin\omega_1 t$. Then the first integral is given by equation (4.18):

$$\int_{t=0}^{T} N_+ \,\mathrm{d}t = -2\pi\omega_1\eta_2 A^2. \tag{4.23}$$

The second integral in (4.22) can be calculated using the fact that for a small dissipation, the interval t_* should be much smaller than T. In this case approximately

$$\int_{t=-t_*/2}^{t_*/2} (N_- - N_+) \,\mathrm{d}t = t_*(N_- - N_+)|_{t=0}. \tag{4.24}$$

For $t = t_*$ it holds that $\dot{z} = v_*$. After substitution $z(t) = A\sin\omega_1 t$ this equality gives $\omega_1 A\cos\omega_1 t_* = v_*$. Keeping in mind that $\omega_1 t_*$ is a small number, one can obtain $v_* \approx \omega_1 A = \dot{z}(0)$. Then the above integral can be calculated as follows:

$$t_*(N_- - N_+)|_{t=0} = 2t_* v_* \lim_{\dot{z}\to v_*+} \left(\frac{f}{m}\right)\bigg|_{z=0} = -2t_* v_* z_*(p_0 + \gamma v_0^2). \tag{4.25}$$

A substitution (4.23) and (4.25) to (4.22) gives

$$\Delta\mathcal{E} = -2\pi\omega_1\eta_2 A^2 - 2t_* v_* z_*(p_0 + \gamma v_0^2) \equiv 0 \quad \Rightarrow \quad t_* = \frac{-\pi\omega_1\eta_2 A^2}{v_* z_*(p_0 + \gamma v_0^2)}. \tag{4.26}$$

A further substitution $A = v_*/\omega_1$ to the above equation finally gives the following formula for the time-interval t_*:

$$t_* = \frac{\pi v_* |\eta_2|}{\omega_1 z_*(p_0 + \gamma v_0^2)}. \tag{4.27}$$

The amplitude of the limit cycle can be calculated as

$$A = \frac{v_*}{\omega_1} = \frac{v_*}{\sqrt{\omega^2 + p_0 + \gamma(v_0 - v_*)^2}}. \tag{4.28}$$

A typical phase plot for the case of small dissipation is shown in figure 21*a*. Figure 21*b* shows a close-up of the area corresponding to the time-interval t_*, where the dry friction force changes its sign, therefore limiting the amplitude of oscillations and causing the formation of a limit cycle. A corresponding time-history for the phase plot is depicted in figure 22.

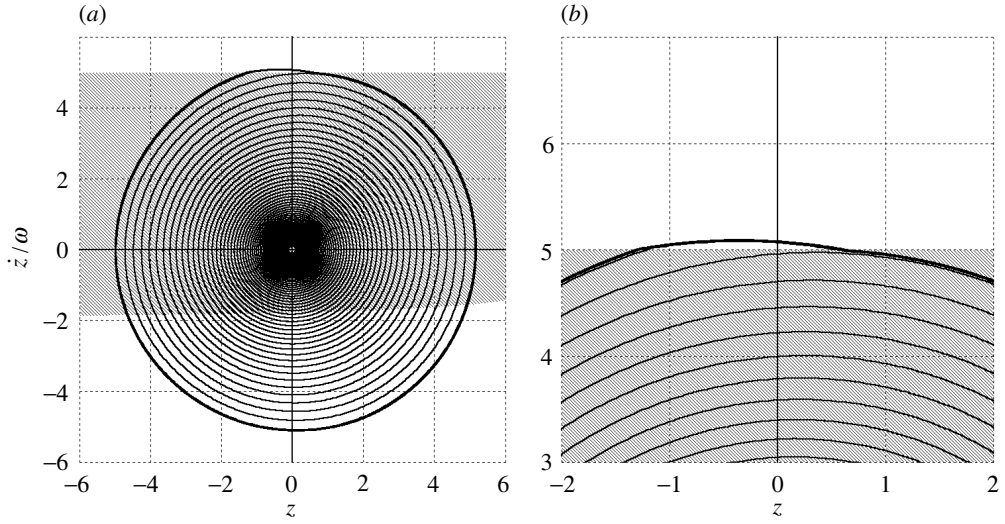

Figure 21. Phase plane for the case of small friction: (*a*) general view, (*b*) close-up of the critical zone.

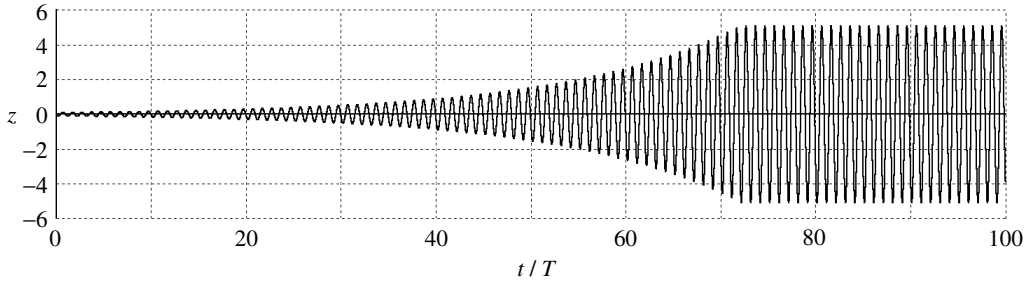

Figure 22. Time-history of the chatter appearance for the case of small friction.

5. Conclusions

In this paper frictional dynamic models of the orthogonal metal cutting generating chatter were examined, where a dry friction force acting on the cutting edge and stochastic properties of the workpiece were introduced. The system demonstrates a complex dynamic behaviour, which is manifested by the existence of periodic, quasi-periodic, subharmonic and chaotic motion. It was found that some of the bifurcation diagrams cannot be classified into standard routes to chaos, however; *crisis type* transition to chaos is dominating. The strong influence of the intermittent cutting and dry friction can produce multidimensional attractors (Wiercigroch 1997).

Two unique nonlinear phenomena were detected. The first one is called *unidirectional bifurcation*, i.e. the system is stable in the one direction and unstable in the other. The *deaths and births* of periodic solutions are the second phenomenon, where the system *oscillates* between the stable and asymptotically stable states as the damping ratio increases (Wiercigroch 1997).

The introduction of stochasticity can cause an immense increase in the cutting forces (up to 300%) during the initial period of cutting. This could explain the industrial reality, where the majority of the catastrophic tool breakage occurs dur-

ing this initial stage. This finding can be valuable for design and control engineers (Wiercigroch & Cheng 1997).

The stability analysis showed that if the optimum velocity for the dry friction force is smaller than the average relative velocity between the tool and the workpiece, then the cutting process is stable. For the case of small friction it was proved that an increase in the depth of cut and the dry friction nonlinearity decrease the stability. Moreover, it was shown that a large viscous friction can always prevent chatter. Another important conclusion is that discontinuous character of the friction force is essential for chatter generation; no chatter can appear in the zone were the friction force is continuous.

In general, it may be concluded that the nonlinear dynamic responses of the system can be controlled most effectively by the cutting force modulus. Contrary to classical machine-tool theory, it has been observed that for certain values of the parameter vector the amplitude of vibration can decrease with an increase in cutting force, which can be used as design information to improve the productivity and accuracy of machine tools.

References

Foong, C. H., Wiercigroch, M. & Deans, W. F. 2001 Experimental study of the nonlinear dynamics of orthogonal metal cutting. *Int. J. Mech. Mech. Engng* **4**. (In the press.)

Grabec, I. 1988 Chaotic dynamics of the cutting process. *Int. J. Mech. Tools Manufact.* **28**, 19–32.

Hastings, W. F., Mathew, P. & Oxley, P. L. B. 1980 A machining theory for predicting chip geometry, cutting forces, etc., from material properties and cutting conditions. *Proc. R. Soc. Lond.* A **371**, 343–354.

Hillber, H. M. & Hughes, T. J. R. 1978 Collocation, dissipation and overshoot for time integration schemes in structural dynamics. *Earthq. Engng Struct. Dyn.* **6**, 99–117.

Kapitaniak, T. 1990 *Chaos in systems with noise*. World Scientific.

Kudinov, V. A. 1963*a* Dynamic characteristics of the metal cutting process. *Stanki i Instrument* **10**, 1–7. (In Russian.)

Kudinov, V. A. 1963*b* *Dynamics of machine tools*. Moscow: Mashinostrojenie. (In Russian.)

Merchant, M. E. 1944 Basic mechanics in the metal cutting process. *Trans. ASME J. Appl. Mech.* **168**, 168–175.

Merchant, M. E. 1945 Mechanics of the metal cutting process: orthogonal cutting and a type 2 chip. *J. Appl. Phys.* **16**, 267–275.

Rice, S. O. 1954 Mathematical analysis and random noise. In *Selected papers on noise and stochastic processes* (ed. N. Wax), pp. 133–294. Dover

Shinozuka, M. & Deodatis, G. 1992 Simulation of stochastic processes by spectral representation. *Appl. Mech. Rev.* **44**, 191–203.

Shinozuka, M. & Jan, C.-M. 1972 Digital simulation of random processes and its applications. *J. Sound Vib.* **25**, 111–128.

Stépán, G. 1998 Delay-differential equation models for machine tool chatter. *Dynamics and chaos in manufacturing processes* (ed. F. C. Moon), pp. 165–191. Wiley

Tlusty, J. 1986 Dynamics of high speed milling. *AMSE J. Engng Industry* **108**, 59–67.

Wiercigroch, M. 1990 Modelling dynamic interactions between machine tool and cutting process. PhD thesis, Silesian University of Technology, Gliwice. (In Polish.)

Wiercigroch, M. 1994 A numerical method for calculating dynamic responses in the machine tool–cutting process system. *Arch. Mech. Engng* **41**, 29–38.

Wiercigroch, M. 1997 Chaotic vibrations of a simple model of the machine tool–cutting process system. *Trans. ASME J. Vib. Acoust.* **119**, 468–475.

Wiercigroch, M. & Cheng, A. D.-H. 1997 Chaotic and stochastic dynamics of metal cutting process. *Chaos, Solitons and Fractals* **8**, 715–726.

Yang, C. Y., Cheng, A. H.-D. & Roy, R. V. 1991 Chaotic and stochastic dynamics for nonlinear structural system with hysteresis and degradation. *Probabilistic Engng Mech.* **6**, 193–203.

Zorev, N. N. 1956 *Questions asked from mechanics of the metal cutting processes*. Moscow: Mashinostrojenie. (In Russian.)